Contents lists available at ScienceDirect

Arabian Journal of Chemistry

journal homepage: www.ksu.edu.sa

Integrated serum, urine metabolomics and 16S rRNA sequencing to investigate the modulatory effect of Ziziphi Spinosae Folium flavonoid on D-galactose-induced aging of rats

Yu Tao [a,1], Cai Fu [a,1], Huizhi Du [a], Chenhui Du [b,*], Yan Yan [a,*]

[a] Modern Research Center for Traditional Chinese Medicine, Shanxi University, Taiyuan 030006, China
[b] School of Traditional Chinese Materia Medica, Shanxi University of Chinese Medicine, Taiyuan 030619, China

ARTICLE INFO

Keywords:
Ziziphi Spinosae Folium flavonoids
Anti-aging
Cognitive dysfunction
Metabolomics
16S rRNA sequencing
"microbiota-gut-brain" axis

ABSTRACT

Ziziphi Spinosae Folium, the leaf of *Ziziphus jujuba* Mill. var. *spinosa* (Bunge) Hu ex H. F. Chou (LZJS), was widely distributed in northern China. Our previous study showed that LZJS flavonoid (LZJSF) exerted antioxidant activity at chemical and PC12 cell levels, respectively. Here, we further studied the function of LZJSF on aging-related oxidative stress in D-galactose (D-gal)-induced rats and the potential mechanisms were explored. The aging model was established by intraperitoneal injection of D-gal (300 mg·kg^{-1}·day^{-1}) for 36 days, the low-dose of LZJSF (LLZJSF 100 mg·kg^{-1}·day^{-1}) and the high-dose of LZJSF (HLZJSF, 200 mg·kg^{-1}·day^{-1}) were administered daily by oral gavage at the same time, respectively. Their spatial and learning memory abilities were evaluated by the Morris water maze test. HLZJSF was observed to significantly ameliorate cognitive ability and oxidative indexes, such as reduction of MDA and augmentation of SOD, GSH-Px, T-AOC and CAT, and the effect of HLZJSF on these indexes was stronger than that of LLZJSF. A precise and well-defined research strategy was successfully applied to screen serum differential metabolites. Furthermore, integrated serum and urine metabolomics showed that the derivations of nine significant differential metabolites could be regulated by administration of HLZJSF, which suggested that the intervention effect of HLZJSF against aging may involve in the amino acid metabolism including D-Glutamine and D-glutamate, alanine, aspartate and glutamate, arginine and proline metabolism and arginine biosynthesis. 16S rRNA sequencing analysis showed that HLZJSF could descend the relative abundance of *Firmicutes* and *Actinobacteria*, as well as the ratio of *Firmicutes/Bacteroidetes*, and increase the relative abundance of *Bacteroidetes* and *Proteobacteria*. Finally, correlation analysis further showed that the beneficial effects of HLZJSF resulted from the regulation of the disturbance of gut microbiota through the "microbiota-gut-brain" axis to affect amino acid metabolism and regulate oxidative stress. This study will provide a foundation for the development and utilization of LZJSF as functional foods and healthy beneficial food products.

1. Introduction

Aging processing is the progression of degenerative changes in tissues and organs of the body as we age, often accompanied by various illnesses, such as cardiovascular disorders and type 2 diabetes, etc. (Sun et al., 2022). Age-related memory and learning impairment were also important characteristics of aging. As reported, the aging process was closely linked to disrupted redox homeostasis and excessive production

Abbreviations: CV, Coefficient of variation; CAT, Catalase; D-gal, D-galactose; FDR, False discovery rate; FC, Fold Change; GSH-Px, Glutathione peroxidase i.p.,; HLZJSF, high-dose LZJSF; Intraperitoneally injected i.g., Intragastric administration; LEfSe, Linear discriminant analysis effect size; LLZJSF, low-dose LZJSF; LZJSF, Ziziphi Spinosae Folium flavonoid; MWM, Morris Water Maze; OPLS-DA, Orthogonal partial least squares-discriminant analysis; PLS-DA, Partial least squares-discriminant analysis; ROS, Reactive Oxygen Species; SOD, Superoxide dismutase; T-AOC, Total antioxidant capacity; MDA, Malondialdehyde; VIP, Variable importance in the projection.

* Corresponding authors at: Modern Research Center for Traditional Chinese Medicine, Shanxi University, Taiyuan 030006, China (Y. Yan). School of Traditional Chinese Materia Medica, Shanxi University of Chinese Medicine, Taiyuan 030619, China (C.H. Du).
E-mail addresses: dch@sxtcm.edu.cn (C. Du), yanyan520@sxu.edu.cn (Y. Yan).
[1] These authors contributed equally to this work.

https://doi.org/10.1016/j.arabjc.2023.105591
Received 14 August 2023; Accepted 25 December 2023
Available online 26 December 2023

of reactive oxygen species (ROS), resulting in genetic material damage and organ metabolic abnormalities (Sun et al., 2023). The "microbiota-gut-brain" axis might be a novel way to study aging systematically. As the human body aged, changes in the gut barrier, absorption and immune function, and various factors led to the destruction of the gut microecological environment (Ahmed et al., 2010). Evidence suggested that changes in gut microbiota composition might affect cognitive ability at multiple levels (Mou et al., 2022). Furthermore, researchers had also found that restoring gut microbiota might delay aging by reducing oxidative stress and cognitive decline (Liu et al., 2022b). Therefore, restoring the balance of the gut environment and delaying the aging process was of great significance for improving the life quality of the elderly.

Ziziphus jujuba Mill. var. *spinosa* (Bunge) Hu ex H. F. Chou (ZJS) was widely distributed in northern China (Du et al., 2020). ZJS fruits and seeds had been used in traditional Chinese medicine for more than 4,000 years. In addition, the leaf of ZJS (LZJS), named *Ziziphi Spinosae Folium*, had been utilized in herbal teas to enhance sleep quality as a by-product derived from the production of ZJS (Zhang et al., 2014). Previous studies found that LZJS were rich in flavonoids, saponins, nucleosides, and other nutrients (Guo et al., 2011, Guo et al., 2013), and thus LZJS had obvious health effects such as sedation, antioxidant and protecting the liver (Bai et al., 2017). In our previous study, the main Ziziphi Spinosae Folium flavonoid (LZJSF) components were identified including rutin, quercetin, kaempferol, catechin and epicatechin and strong antioxidant activity *in vitro* was proved at different levels (Yan et al., 2020). Rutin, accounted for 3% of LZJS, had been reported to attenuate the senescence effect in D-galactose (D-gal) aging mouse model and protect against aging-related metabolic dysfunction (Yang et al., 2012, Li et al., 2016). Therefore, it was meaningful to study the anti-aging effect and mechanism of LZJSF.

In the study, first, a classic aging rat model, D-gal-induced aging rat model, was applied. Then, the spatial and learning memory abilities of LZJSF were investigated by the Morris water maze test.

Then, ^{1}H NMR metabolomics combined with multivariate statistical methods was used to analyze the changes and metabolic pathways of LZJSF on endogenous metabolites in serum and urine of D-gal-induced aging rats. Furthermore, differential gut microbiota related to D-gal-induced aging and the effect of LZJSF on gut microbiota were investigated by 16S ribosomal RNA (16S rRNA). Finally, correlation analysis was applied to investigate whether its mechanism against aging was relevant to the "microbiota-gut-brain" axis. The findings of this study will establish a solid groundwork for the development and utilization of LZJSF as functional foods and health-promoting food products.

2. Materials and methods

2.1. Chemicals and regents

D-gal was purchased from Sigma-Aldrich (MO, USA). D_2O was purchased from Norell-Landisville Co. (NJ, USA). The superoxide dismutase (SOD), total antioxidant capacity (T-AOC), malondialdehyde (MDA), glutathione peroxidase (GSH-Px) and catalase (CAT) assay kits were purchased from Jiancheng Bioengineering Institute (Nanjing, China). The kits for determination of BCA protein concentration were purchased from Beyotime Institute of Biotechnology (Shanghai, China).

The reference standards of quercetin, quercetin-*3*-*O*-robinobioside (Rob), rutin, quercetin-*3*-*O*-*β*-*D*-glucoside (Glu), quercetin-*3*-rhamnoside (Rha), and quercetin-*3*-*O*-*β*-*D*-galactose (Gal), were purchased from the Herbest Bio-technology Co. (Shaanxi, China).

LZJS was collected from Yuci, Shanxi, China in June 2017, and was authenticated by Prof. Chenhui Du (Shanxi University of Chinese Medicine, Shanxi, China). LZJSF was prepared according to the report by our group. The preparation method of LZJSF was listed in Supplementary File 1. The content test of LZJSF was performed using our previous method (Yan et al., 2020) and the detailed conditions were listed in Supplementary File 2.

2.2. Animal experimental design and sample collection scheme

A total of 36 adult male Sprague-Dawley rats (7 weeks old, weighing 180 ± 20 g) were procured from Beijing Vital River Laboratory Animal Technology Co., Ltd. with License No. SCXK 2016–0006 (Beijing, China). The rats were housed under controlled conditions of temperature (22 ± 2 °C), light (12 h light/dark cycle) and humidity (50 ± 10%). All animal care and experimental procedures were in compliance with the Guidelines for Care and Use of Laboratory Animals of Shanxi University (Approval number. SXULL 2020029; Time: 03/01/2020).

Following one-week acclimatization to their home cages, the rats were randomly divided into 4 groups (9 rats per group) and treated with normal saline (Control group), 300 mg/kg of D-gal (D-gal group), 300 mg/kg of D-gal plus 100 mg/kg of LZJSF (the low-dose LZJSF, named as LLZJSF) group and 300 mg/kg of D-gal plus 200 mg/kg of LZJSF (the high-dose LZJSF, named as HLZJSF) group. The D-gal group was intraperitoneally injected (i. p.) with D-gal once daily for 36 consecutive days, while the Control group received the same dosage of normal saline. Then, the two drug groups were administered with LZJSF which was dissolved in distilled water by intragastric administration (i. g.) 1 h after D-gal was injected. After 30 days of feeding, Morris Water Maze (MWM) tests were conducted in each group as previously described to determine each rat's memory capacity (Mifflin et al., 2021). The detailed processes of behavioral analysis via the MWM are described in the Supplementary File 3. Animal experimental design and sample collection scheme are shown in Fig. 1A. The rats were weighed weekly. After 35 days of LZJSF administration, the urine samples and the feces samples were collected individually and stored at −80 °C for further use. The probe test was conducted on the 36 th day, and all rats were sacrificed 1 h after the completion of the probe test. Rat blood obtained from the abdominal aorta was centrifuged at 1,123 × *g* (4 ℃) for 15 min in order to obtain serum samples. Whole brain tissues were collected, immediately weighed and stored at −80 °C for further analysis.

2.3. Measurement of antioxidant indexes in serum and brain

Brain tissues samples were prepared by homogenate and centrifugal treatment at 367 × *g* (4 ℃) for 15 min. The GSH-Px, SOD, MDA, CAT, and T-AOC levels in serum and brain samples were measured with ELISA according to instructions, respectively.

2.4. ^{1}H NMR-based metabolomics analysis

Each serum sample (200 μL) was mixed with 400 μL of D_2O and centrifuged (15, 490 × *g*, 4 °C, 20 min), and then the supernatant was used for NMR analysis on a Bruker 600 MHz AVANCE III NMR spectrometer (Karlsruhe, Germany). Each urine sample was mixed with 100 μL of D_2O and centrifuged (13,200 × *g*, 4 ℃, 10 min) to obtain supernatants for NMR analysis. The serum and urine samples were analyzed using the Carr-Purcell-Meiboom-Gill (CPMG) spinecho pulse sequence consisting of 64 scans with the following parameters: spectral width of 12,019.23 Hz, spectral size of 32,000 data points, and relaxation time of 1.0 s. The specific methods for the ^{1}H NMR spectra processing are in Supplementary File 4.

2.5. Multivariate analysis

For multivariate analysis, all preprocessed NMR data were imported into the Simca-P14.0 software (Umetrics, Sweden). Partial least squares discriminant analysis (PLS-DA) model was applied to examine the trend of changes in serum and urine samples among four groups. For urine sample, the orthogonal projection to partial least square (OPLS-DA) model qualities were determined by examining the total explained variables (R^2X) and predictability (Q^2) values, followed by rigorous

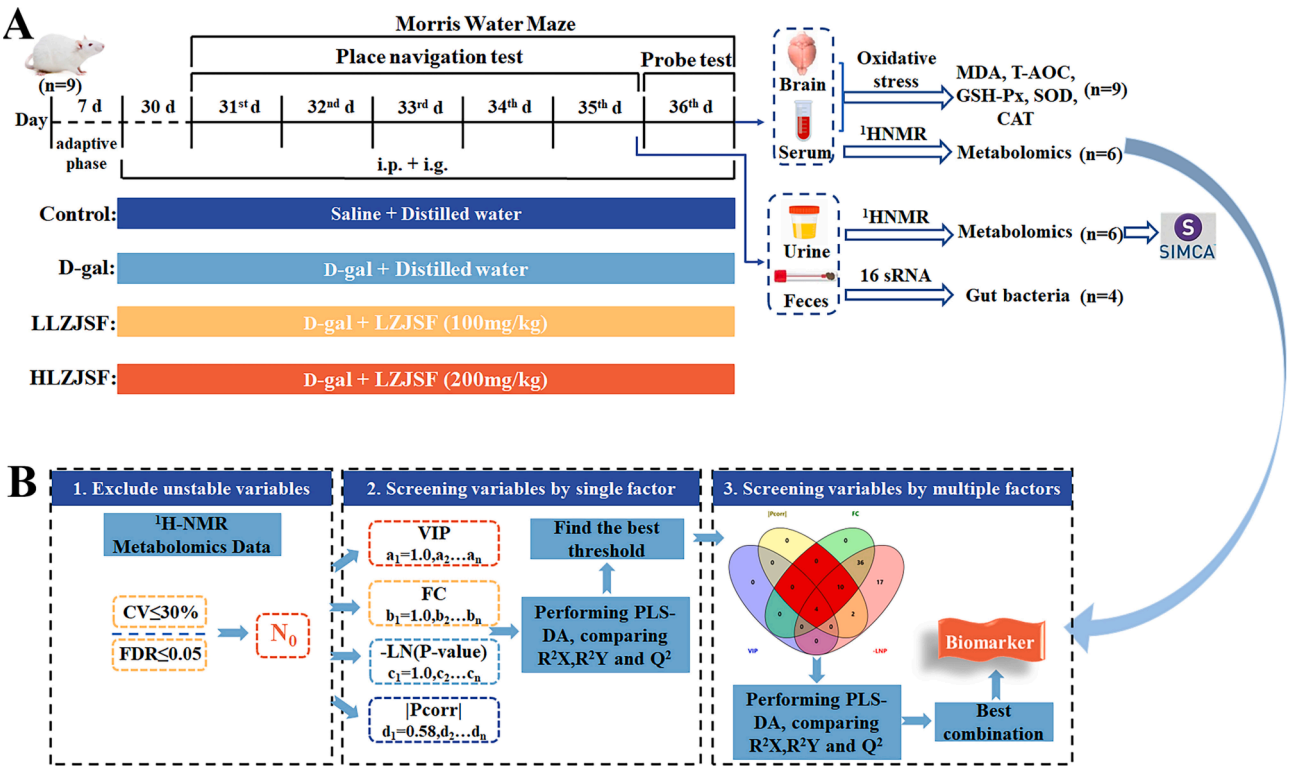

Fig. 1. (A) Animal experimental design and sample collection scheme. (B) Precise and well-defined research strategy for screening different metabolites for serum samples.

permutations (number: 200).

2.6. Precise and well-defined research strategy for screening different metabolites for serum samples

For serum samples, the different metabolites were screened between Control and D-gal group using a precise and well-defined research strategy based on the previous method with minor modification (Li et al., 2019a). In brief, the detailed chart is shown in Fig. 1B and the strategy contained four steps: (1) the variables which met CV (coefficient of variation) ≤ 30 % and the FDR (false discovery rate) ≤ 0.05 were considered as preliminary variables (N_0); (2) the regression equation for $N_a/N_0 = f(a)$, $N_b/N_0 = f(b)$, $N_c/N_0 = f(c)$ and $N_d/N_0 = f(d)$ was conducted, respectively, using the values for four factors including VIP (Variable importance in the projection), FC (Fold Change), -LNP and |Pcorr|. The thresholds of four factors were set as a, b, c and d, respectively. According to VIP > 1, |Pcorr| > 0.58, FC > 1 and -LNP > 3, the minimum values of a, b, c and d were set as $a_{min} = 1$, $b_{min} = 1$, $c_{min} = 3$ and $d_{min} = 0.58$, respectively. The maximum value of a, b, c, d was set as $a_{max} = f^{-1}(N_a/N_0 = 0.01)$, $b_{max} = f^{-1}(N_b/N_0 = 0.01)$, $c_{max} = f^{-1}(N_c/N_0 = 0.01)$, $d_{max} = f^{-1}(N_d/N_0 = 0.01)$, respectively. Each factor was divided equally into 5 thresholds (a_1, a_2, …a_5; b_1, b_2, …b_5; c_1, c_2, …c_5; d_1, d_2, …d_5). The different metabolites were identified based on thresholds from each factor; (3) the different metabolites were further verified by performing PLS-DA analysis. The R^2X, R^2Y and Q^2 were used to evaluate interpreting, grouping and predicting abilities of the model, respectively and the optimal threshold was selected; (4) the above four factors were randomly combined to obtain 11 variable sets which was verified by PLS-DA analysis using the values of R^2X, R^2Y and Q^2, respectively. Finally, the significant different metabolites were obtained.

2.7. Gut microbiota sequencing analysis

16S rRNA gene sequencing analysis of feces samples was performed by Shanghai Personal Biotechnology Co., Ltd. (Shanghai, China) using the Illumina Miseq platform (2 × 300 bp paired end runs). Sequence reads was processed using QIIME (version 1.8.0). The data analysis was conducted using the Genes Cloud platform (https://www.genescloud.cn).

2.8. Statistical analysis

All experimental values represented the mean ± standard deviation (SD). The illustrations were created using GraphPad Prism version 8.0 (Graph Pad). Statistical differences between two groups were performed using *t*-test on SPSS 19.0 (New York, USA). Spearman's correlation analysis and visualization were performed using the Chiplot platform (https://www.chiplot.online). The generation of a network graph was facilitated through the utilization of Cytoscape 3.7.2. Metabolic pathways and related metabolites were analyzed using the KEGG database (https://www.kegg.com). Potential markers and ^{1}H NMR data were identified by using BMRB (https://bmrb.io) and HMDB (https://www.hmdb.ca).

3. Results

3.1. Determination contents of six component in LZJSF

The contents of quercetin-*3*-*O*-Rob, rutin, quercetin-*3*-*O*-*β*-*D*-Gal, quercetin-*3*-*O*-*β*-*D*-Glu, quercetin-*3*-Rha, and quercetin of LZJSF were measured by LC-MS/MS according to the method reported in our group (Yan et al., 2020), with 0.83%, 0.010%, 0.030%, 0.020%, 0.00050%, and 1.00%, respectively (Fig. S1).

3.2. Effect of LZJSF on cognitive dysfunction in D-gal-induced aging rats

To address whether LZJSF displayed aging-induced cognitive dysfunction, D-gal-induced aging rats in the present study were used as

aging models. Rats were tested for spatial learning and hippocampal-dependent memory using MWM tests. As shown in Fig. 2A, all groups gradually decreased their escape latency. Specially, rats in the D-gal group found the platform significantly slower than those in the Control group on day 5 ((26.00 ± 1.12) s *vs.* (20.00 ± 5.99) s, $P < 0.001$). Meanwhile, the HLZJSF group shortened significantly escape latency in the spatial learning-memory test compared to the D-gal group on day 5 ((20.44 ± 2.56) s *vs.* (26.00 ± 1.12) s, $P < 0.05$), while the escape latency of LLZJSF group tended to shorten with no significant difference ((26.00 ± 1.12) s *vs.* (22.61 ± 5.29) s, $P > 0.05$). In addition, the swimming speed of HLZJSF group rats was significantly accelerated (Fig. 2B). In the spatial probe test, the HLZJSF significantly increased the distance and time in the target quadrant as well as the number of platform crossings in the aging rats compared to the D-gal group. (Fig. 2C, D). These results indicated HLZJSF had the protective effect on age-induced decline in spatial memory capacity.

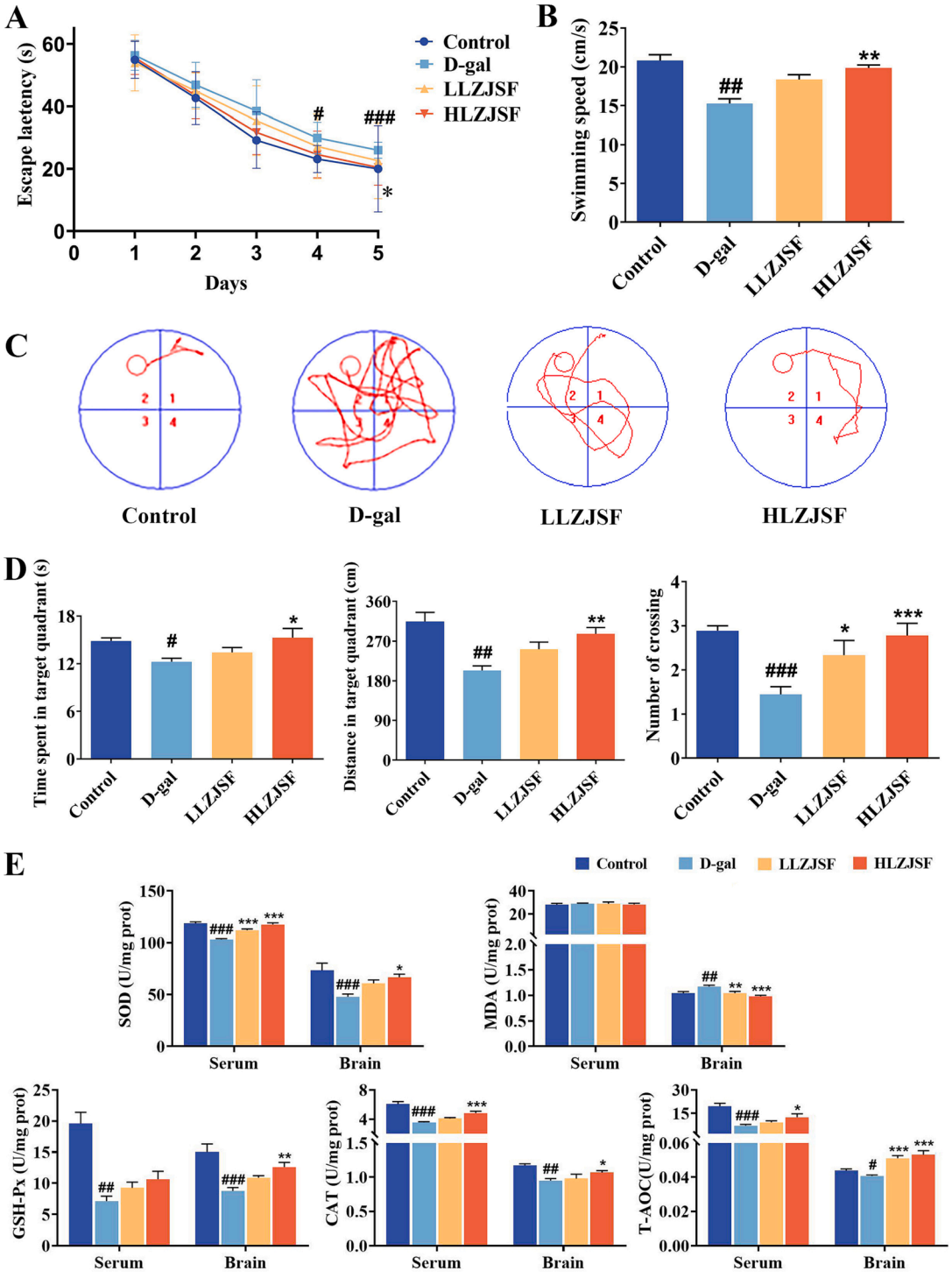

Fig. 2. Effects of LZJSF on cognitive impairment and oxidative stress in D-gal-induced aging rats. (A) Escape latency and (B) Swimming speed of each group of rats; (C) Swimming paths of representative rats in each group. (D) Time spent in target quadrant; distance in the target quadrant; and the number of platform crossings in 60 s in the spatial probe test. (E) Effects of LZJSF on the levels of SOD, MDA, GSH-Px, CAT and T-AOC in brain and serum. Data represent the mean ± SD (n = 9/group). $^{\#}P < 0.05$, $^{\#\#}P < 0.01$, $^{\#\#\#}P < 0.005$, compared to the Control group; $^{*}P < 0.05$, $^{**}P < 0.01$, $^{***}P < 0.001$, compared to the D-gal group.

3.3. Effect of LZJSF on oxidative stress in D-gal induced aging rats

In comparison to the Control group, the D-gal group rats had a significant decrease in SOD ($P < 0.001$), GSH-Px ($P < 0.001$), T-AOC ($P < 0.05$) and CAT ($P < 0.01$) contents in the brain, while a significant increase in the MDA levels ($P < 0.01$), indicating that the D-gal group rats had oxidative damage in the brain (Fig. 2E). Meanwhile, a protective effect of HLZJSF was observed against D-gal-induced brain damage, supported by significantly higher SOD ($P < 0.05$), GSH-Px ($P < 0.01$), T-AOC ($P < 0.001$) and CAT ($P < 0.05$) level and lower MDA in brain ($P < 0.001$). LLZJSF group exhibited a recovery trend in SOD, GSH-Px and CAT level, but only the effects on MDA ($P < 0.01$) and T-AOC ($P < 0.001$) had significant difference. Except for MDA and GSH-Px, the profiles of antioxidant-related indicators in the serum were consistent with those in the brain after administration of HLZJSF. These results suggested that the intake of LZJSF significantly improved the antioxidant ability in D-gal-induced aging mice. Notably, stronger effects at the HLZJSF group than at LLZJSF were observed, which was consistent with

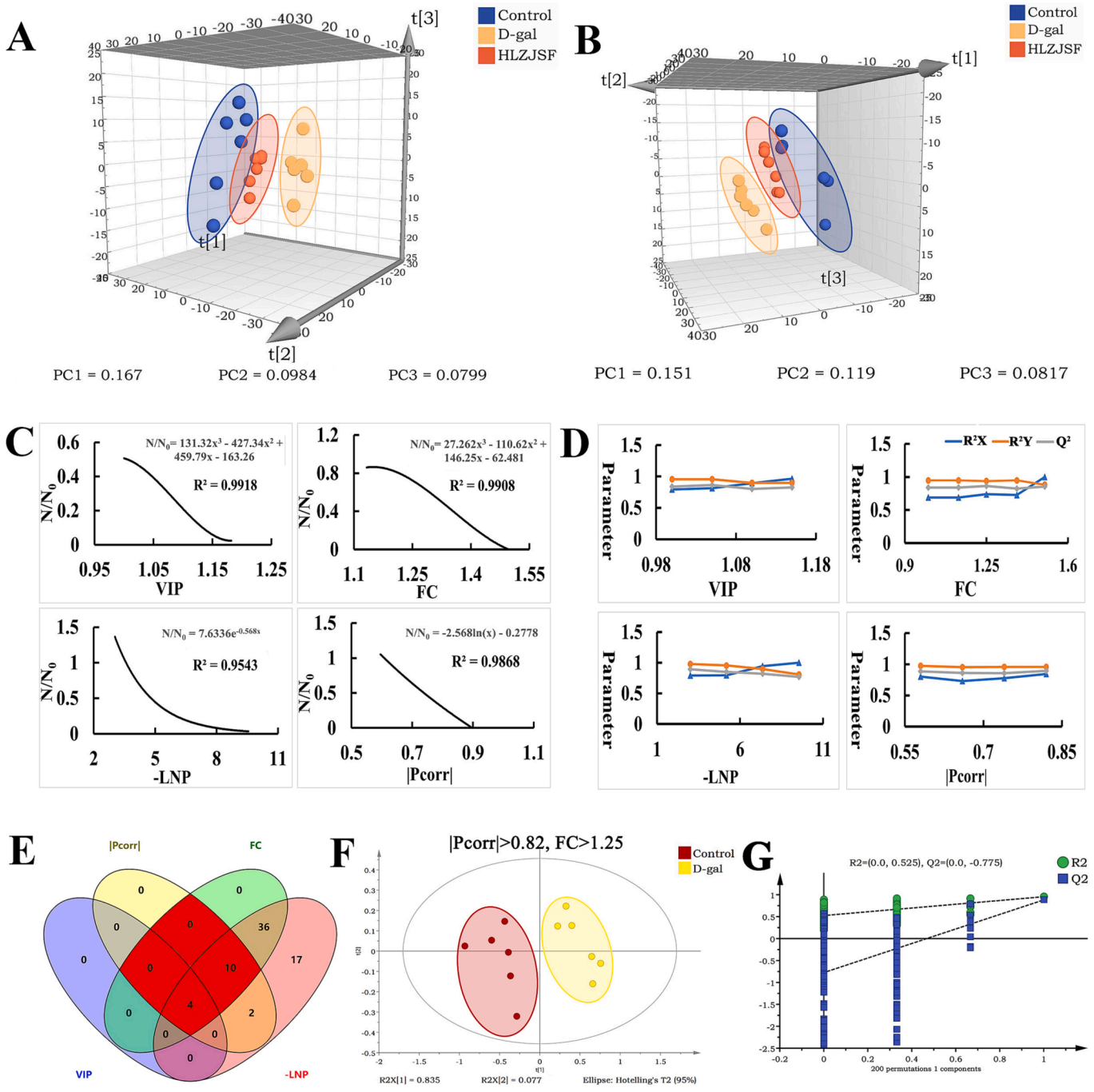

Fig. 3. Multiple statistical analysis from ^{1}H NMR spectra. PLS-DA 3D score plots of the serum samples (A) and the urine samples (B). The regression curves for N/N_0 (Ratio of the number of variables satisfying the factor threshold to the number of preliminary variables) and factor thresholds (VIP, FC, -LNP and |Pcorr|) in serum samples (C). Variables were screened by single factor in serum samples: the R^2X, R^2Y, and Q^2 of the PLS-DA model were performed on the variable sets selected by screening the thresholds of VIP, FC, -LNP and |Pcorr|, respectively (D). The Venn plots of the variable meeting the requirements of combined factors in serum. The optimal combination of factors for screening biomarkers was marked in red (E). The scores plot of PLS-DA models performed by the best combination of factors in serum samples(F). The best combination was tested by PLS-DA model permutation (G). (n = 6).

the behavioral results above. Thus, HLZJSF group was selected for further mechanism study.

3.4. Serum and urine metabolomics study

3.4.1. Effect of HLZJSF on serum and urine metabolic profiles

The urine samples on the 35th and serum samples on the 36th collected from each group were analyzed by ^{1}H NMR, respectively. The typical ^{1}H NMR spectra of the serum and the urine of Control group, D-gal group and HLZJSF group rats are shown in Fig. S2A and S2B, respectively. The chromatograms of the three serum groups displayed negligible disparity, despite variations in peak intensities. Similar results were found in three groups of urine samples. Based on the unique chemical shifts and the coupled constants of the compounds, 30 serum metabolites and 30 urine metabolites were tentatively identified through the integration references, HMDB (Human Metabolome Database) and RMRB (Biological Magnetic Resonance Bank) databases, respectively. The detailed information is listed in Table S1 and Table S2.

By firstly using of PLS-DA 3D score plot (Fig. 3A), the metabolic profile of rats in the D-gal group deviated from that of the Control group, indicating that D-gal induced significant biochemical changes in the rats. The metabolic profiles in the HLZJSF group exhibited significant differences compared to those in the D-gal group, but were similar to those in the Control group. For urine sample, the similar results were observed in HLZJSF treated group, which was close to the Control group with apparent classification from D-gal group (Fig. 3B).

3.4.2. Identification of potential serum and urine biomarkers in D-gal-induced aging rats

To discern more subtle metabolic variances between the Control and D-gal groups from serum samples, the precise and well-defined research strategy mentioned above was applied. Totally, 69 variables meeting CV $\leq$ 30 % and FDR $\leq$ 0.05 were obtained as preliminary variables (N_0), and the values of VIP, FC, -LNP and |Pcorr| were calculated from N_0 using linear regression equations as follows, respectively.

$$N_a/N_0 = 131.32x^3 - 427.34x^2 + 459.79x - 163.26 \quad R^2 = 0.9918 \tag{1}$$

$$N_b/N_0 = 27.262x^3 - 110.62x^2 + 146.25x - 62.481 \quad R^2 = 0.9908 \tag{2}$$

$$N_c/N_0 = 7.6336e^{-0.568x} \, R^2 = 0.9543 \tag{3}$$

$$N_d/N_0 = -2.568\ln(x) - 0.2778 \, R^2 = 0.9868 \tag{4}$$

As shown in Fig. 3C, the R^2 values of the regression equations from VIP, FC, -LNP and |Pcorr| were all greater than 0.95, accurately reflecting the change in N_a/N_0, N_b/N_0, N_c/N_0 and N_d/N_0 (Liu et al., 2023a). According to linear regression equations, the maximum values for a, b, c and d were calculated as 1.19, 1.5, 11.72, 0.9, respectively. In addition, each variable had 5 thresholds (Table 1).

Subsequently, PLS-DA analysis was further performed to screen the best thresholds of the four factors based on the R^2X, R^2Y and Q^2 values. Firstly, the best thresholds for a, b, c, and d were calculated as 1.15, 1.25, 3, and 0.82, respectively (Fig. 3D). Secondly, a total of 11 variables sets were obtained according to the 11 combinations of factors (Fig. 3E). The number of the variables of *Number 1*, *2*, *3*, *7*, *8*, *9* and *11*; *Number 4* and *Number 10* were the same, respectively (Table 2). Thirdly, the R^2X, R^2Y, and Q^2 values of *Number 1* (or *Number 2*, *3*, *7*, *8*, *9* and *11*), *Number 4* (or *Number 10*), *Number 5, Number 6* were calculated. As shown in Fig. S3, the highest values of R^2X, R^2Y, and Q^2 from different variables sets were observed. Furthermore, the optimal combination of *Number 4* (or *Number 10*) was obtained (Fig. 3F) through the sum of R^2X, R^2Y, and Q^2 and 14 variables were further verified by permutation test (number: 200) (Fig. 3G). Therefore, *Number 4* (or *Number 10*) was selected as the best combination of factors to expect biomarkers. Finally, 6 significantly differential serum metabolites, including leucine, valine, isoleucine, arginine, lysine and glutamate from the corresponding variables sets, were identified.

A supervised OPLS-DA model with validation parameters of fitness and predictability in Control *vs.* D-gal was conducted for urine sample (Fig. S4A). As shown in Fig. S4B, OPLS-DA model had R^2 value of 0.995 and Q^2 value of −0.367 after 200 permutations, indicating that the model had no over-fitting phenomenon and reliable for subsequent analysis. Totally, 6 differential metabolites including leucine, creatinine, hippurate, xanthine, alanine and glutamine, were identified from the corresponding S-plot based on VIP > 1 and $P < 0.05$ (Fig. S4C).

3.4.3. Effect of HLZJSF on the altered serum and urine metabolites and metabolic pathway in D-gal-induced aging rats

The variation tendency of the identified potential serum metabolites was compared among the three experimental groups using a one-way ANOVA. As shown in Fig. 4A, a significant increase in leucine, valine, isoleucine, arginine, lysine and glutamate was observed in the D-gal group compared to the Control group. Conversely, HLZJSF could remarkably reverse the abnormities of those six serum metabolites. For urine sample, the D-gal group had significant reductions in leucine, creatinine and glutamine, while a significant increase in the xanthine, alanine and hippurate levels compared to the Control group (Fig. S4D). The deviations induced by D-gal of xanthine, alanine and hippurate were corrected with HLZJSF treatment.

Subsequently, perturbed metabolic pathways in response to D-gal-induced-aging were mapped on KEGG (impact values > 0.1). As shown in Fig. 4B, six serum metabolites were involved into four different metabolic pathways in D-gal-induced aging rats, namely D-Glutamine and D-glutamate, alanine, aspartate and glutamate, arginine and proline metabolism, as well as arginine biosynthesis. Six potential urine metabolites in D-gal-induced aging rats involved in D-Glutamine and D-glutamate, alanine, aspartate and glutamate metabolism and arginine biosynthesis (Fig. 4C). Meanwhile, the analysis revealed that HLZJSF intervention in the D-gal-induced-aging model rats targeted four serum metabolic pathways and three urine metabolic pathways, respectively (Table S3).

Finally, an integrated serum and urine metabolic pathways in aging rats associated with HLZJSF were further investigated. As shown in Fig. 4D, a holistic network map was constructed according to the KEGG

Table 1
Thresholds and the number of variables for each factor.

N_0	VIP		FC		-LNP		|Pcorr|	
	a	Na	b	Nb	c	Nc	d	Nd
69	1.00	36	1.00	63	3.00	69	0.58	67
	1.05	26	1.13	63	5.18	34	0.66	53
	1.10	15	1.25	50	7.36	5	0.74	36
	1.15	4	1.38	22	9.54	1	0.82	16
	1.19	0	1.50	2	11.72	0	0.90	0

Note: Na, Nb, Nc and Nd were the number of variables selected through the threshold range, respectively.

Table 2
The arranged and combined variable and number of the variables.

Number	Combination	Number of the variables
1	VIP, |Pcorr|	4
2	VIP, FC	4
3	VIP, -LNP	4
4	|Pcorr|, FC	14
5	|Pcorr|, -LNP	16
6	FC, -LNP	50
7	VIP, |Pcorr|, FC	4
8	VIP, |Pcorr|, -LNP	4
9	VIP, FC, -LNP	4
10	|Pcorr|, FC, -LNP	14
11	VIP, |Pcorr|, FC, -LNP	4

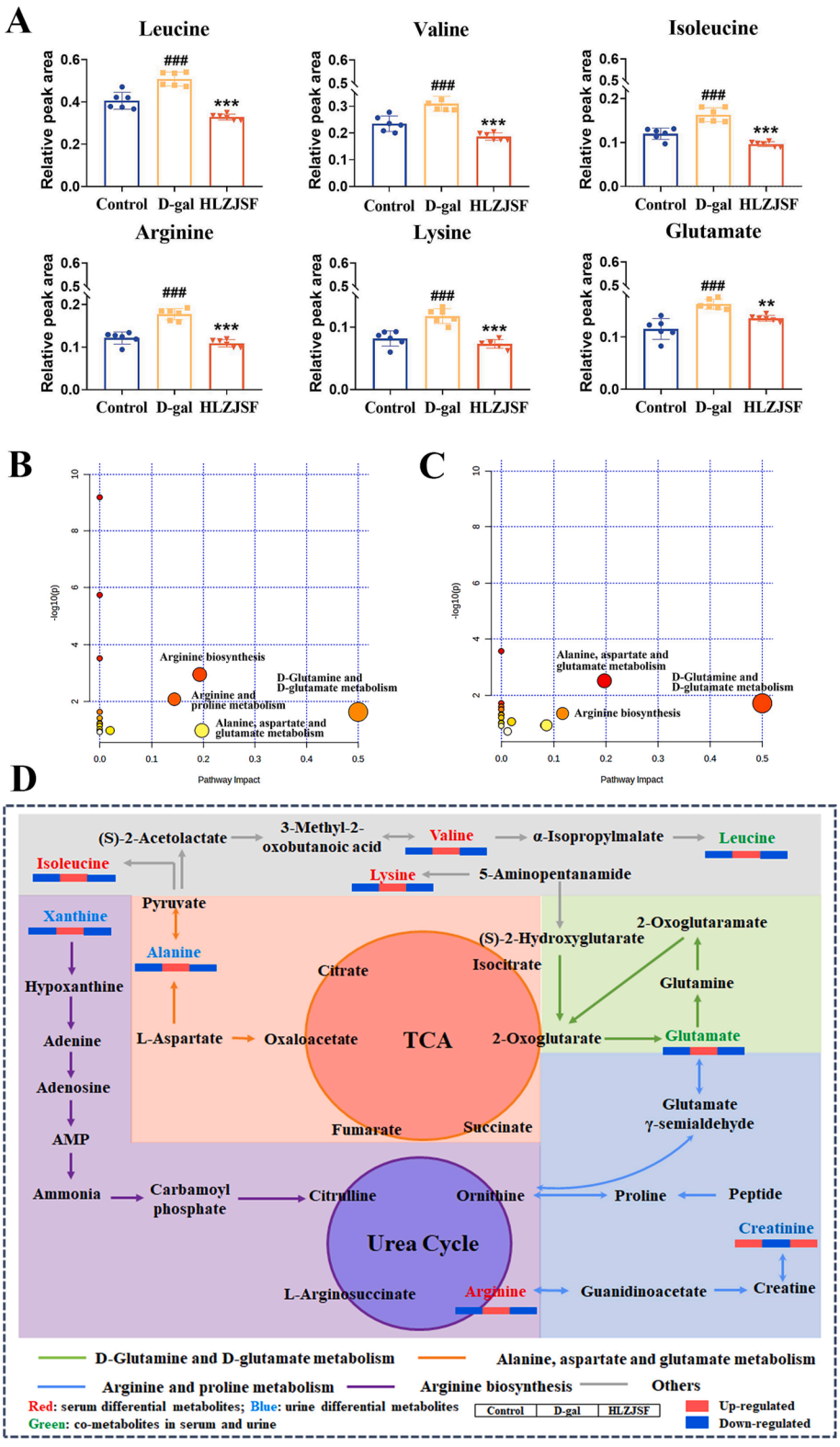

Fig. 4. (A) Comparison of the relative intensity of potential biomarkers in the aging rats associated with HLLZSF treatment. $^{\#}P < 0.05$, $^{\#\#}P < 0.01$, $^{\#\#\#}P < 0.005$, compared to the Control group; $^{*}P < 0.05$, $^{**}P < 0.01$, $^{***}P < 0.001$, compared to the D-gal group. (B) Serum metabolic pathways of D-galactose rats compared with control rats as visualized by bubble plots. Bubble size is proportional to the impact of each pathway and bubble color denoting the significance from highest in red to lowest in white. (C) Urine metabolic pathway analysis of D-galactose rats compared with control rats as visualized by bubble plots. (D) The holistic metabolic network map of the differential metabolites in serum and urine according to the KEGG PATHWAY database (n = 6). Metabolite names in green, red and blue mean they were detected in both serum and urine, only in serum and only in urine, respectively.

(https://www.kegg.com) and references (Zhao et al., 2020). Notably, treatment with HLZJSF regulated nine differential metabolites involved in the four altered metabolic pathways.

3.5. Effect of HLZJSF on the regulation of gut microbiota structure

Accumulating reports pointed that gut microbiota dysbiosis and aging were interconnected (Chen et al., 2018). To further demonstrate the crucial role of the gut microbiota in mediating aging induced cognitive dysfunction, the study of the intake of HLZJSF on the gut

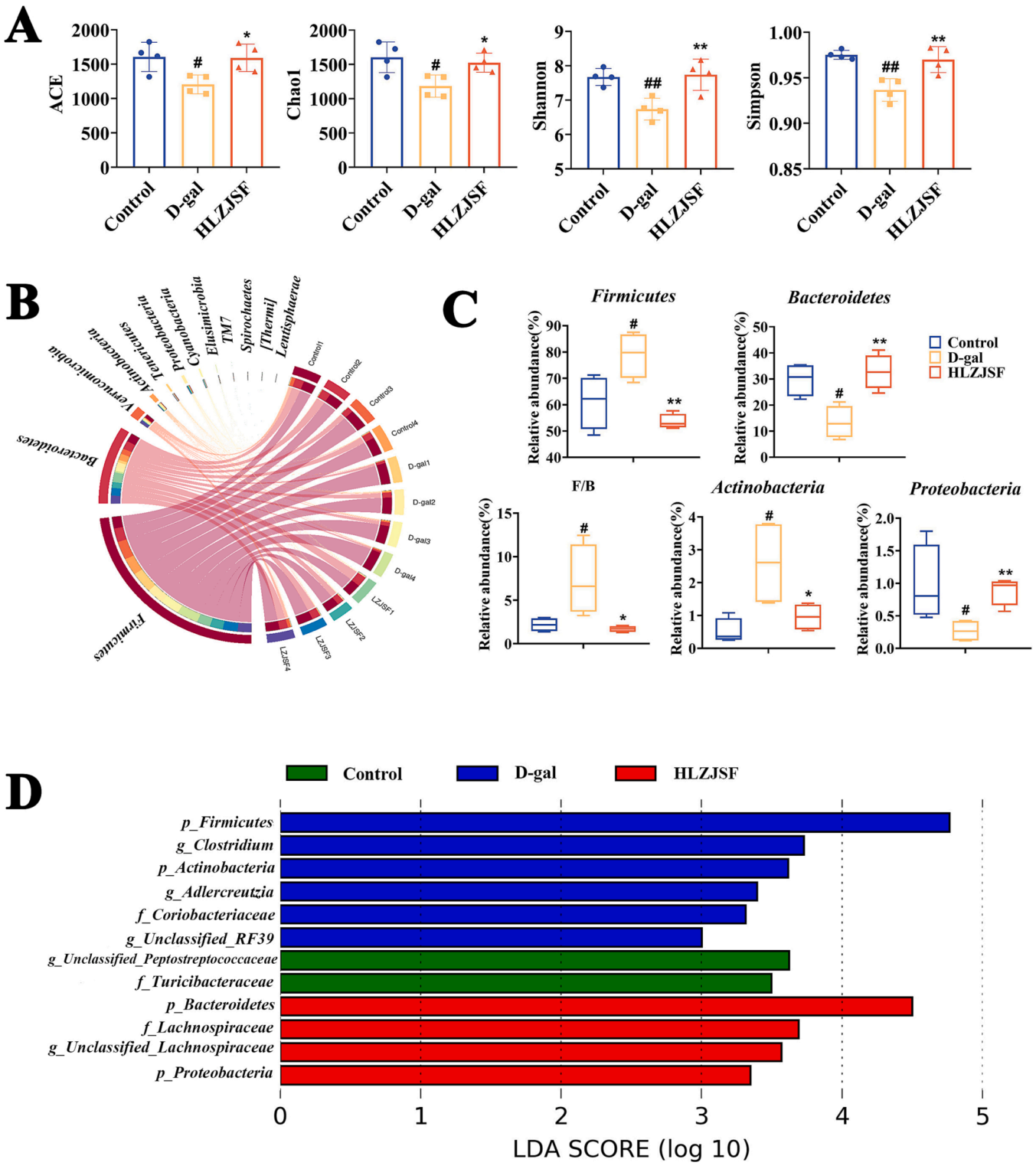

Fig. 5. Analysis of the diversity, composition and differences of gut microbiota in feces samples. (A) Alpha diversity indexes in each group. (B) Circos plot showing gut microbiota taxonomic profiling at the phylum level in three groups. (C) The relative abundance of major gut microbiota at the phylum level; F/B represents the ratio of *Firmicutes*-to-*Bacteroidetes*. $^{\#}P < 0.05$, $^{\#\#}P < 0.01$, $^{\#\#\#}P < 0.005$, compared to the Control group; $^{*}P < 0.05$, $^{**}P < 0.01$, $^{***}P < 0.001$, compared to the D-gal group. (D) LEfSe analysis of bacterial taxa (n = 4). Histogram of LDA displayed the most enriched bacterial taxa in each group (LDA score threshold > 2.0).

microbiome in rats with cognitive dysfunction was performed. A total of 908,263 sequences were gained among three group by high-throughput sequencing. The results demonstrated that both the Rarefaction and Shannon index curves approached the saturation plateau, revealing that high coverage of approximately 99% was attained in all samples (Fig. S5A). The ACE, Chao1, Shannon and Simpson indexes were used to analyze the alpha diversity of gut microbiota. Compared with the Control group, ACE, Chao1, Shannon and Simpson index were significantly decreased in D-gal group, indicating a lower microbiota community diversity induced by D-gal (Fig. 5A). The intake of HLZJSF largely restored the gut microbiota α-diversity. To better compare microbiota community differentiation among the three groups, PLS-DA score plot was performed on the OTU abundance. As shown in Fig. S5B, the Control and D-gal groups were clearly separated. The HLZJSF group was positioned between Control and D-gal groups, in close proximity to the Control group, suggesting that HLZJSF could restore gut microbiome disorders in D-gal-induced aging rats. These findings implied that HLZJSF could improve microbial diversity and uniformity.

At the phylum level, *Firmicutes*, *Bacteroidetes*, *Verrucomicrobia*, *Actinobacteriota* and *Proteobacteria* were the dominant microbiota in the rat feces of three groups (Fig. 5B). HLZJSF administration resulted in the reduction of the relative abundance of *Firmicutes*, *Actinobacteriota* and an increase in *Bacteroidetes* and *Proteobacteria* abundance compared to D-gal group, as shown in Fig. 5C. In addition, the HLZJSF group exhibited a significant increase in *Firmicutes/Bacteroidetes* (F/B) ratios compared to the D-gal group. At the family level, the abundant microbiota taxa among the three groups included *Lactobacillaceae, Unclassified_Clostridiales, S24-7, Ruminococcaceae, Prevotellaceae, and Verrucomicrobiaceae* (Fig. S6A). Meantime, we observed that a greater relative abundance of *Lactobacillaceae* and a lower relative abundance of *S24-7* in the D-gal group compared to the Control group. With HLZJSF administration, the abundances of *Lactobacillaceae* and *S24-7* were dramatically reduced and enhanced, respectively (Fig. S6B).

Furthermore, LEfSe analysis was also used to analyze gut microbiota diversity among different groups. The histogram of LDA revealed that the presence of 12 distinct gut microbiota, including *p_Firmicutes*, *p_Bacteroidetes*, *p_Actinobacteria*, *p_Proteobacteria*, *f_Coriobacteriaceae*, *f_Lachnospiraceae*, *f_Turicibacteraceae*, *g_Unclassified_Peptostreptococcaceae*, *g_Clostridium*, *g_Unclassified_Lachnospiraceae*, *g_Adlercreutzia* and *g_Unclassified_RF39* (Fig. 5D).

3.6. Correlation analysis between key bacterial taxa and host parameters

Spearman correlation analysis was conducted to examine the relationship between changes in gut microbiota composition and age-related characteristics, using a significance threshold of $|r| > 0.5$ and $P < 0.05$. As shown in Fig. 6A, the main altered genera belonging to the phylum *Firmicutes* were found to be highly associated with swimming speed of aging rats in MWM test. More specially, a significantly negative correlation was observed between *Clostridium* (members of phylum *Firmicutes*), *Actinobacteria* and swimming speed.

Additionally, certain differential genera assigning to the phylum *Firmicutes* (member of genus *Clostridium*) and *Actinobacteria* exhibited significant negative correlation with brain oxidative indexes (GSH-Px, CAT and T-AOC). In contrast, positive correlations were presented with brain MDA. In addition, the relative abundance of *Bacteroidetes* were positively correlated with brain SOD, GSH-Px and T-AOC, while negative correlations were observed with brain MDA. *Bacteroidetes, Proteobacteria* and *Unclassified_Lachnospiraceae* showed strong positive associations with differential metabolites (such as leucine, valine, isoleucine, arginine, lysine and glutamate), whereas *Firmicutes* and *Unclassified_RF39* showed the opposite correlation. Notably, glutamate was significantly associated with the eleven key bacterial taxa except for *Turicibacteraceae* (members of phylum *Firmicutes*). Twelve key bacterial taxa, two phenotypes, five brain oxidative indexes and nine differential metabolites were integrated into the network, respectively (Fig. 6B).

4. Discussion

In the study, LZJSF was investigated to effectively mitigate cognitive dysfunction in D-gal-induced aging rats via the microbiota-gut-brain axis.

4.1. LZJSF mitigated cognitive dysfunction in D-gal-induced aging rats

Numerous studies had demonstrated that aging was accompanied by a decline in memory and cognitive abilities (Ruan et al., 2013). Consistent with a previous study (Li et al., 2023a), we observed that D-gal-induced aging rats had a significant reduction of the swimming speed, time and distance in the target quadrant and the number of platform crossings in the MWM test, indicating that D-gal impaired memory and cognition in aging rats. HLZJSF significantly increased all the aforementioned indexes and showed beneficial effects in mitigating cognitive dysfunction, which provided new evidence to reveal candidate bioactive compounds by which LZJS regulated aging. Previous studies had shown that aging was closely related to oxidative stress (Ionescu-Tucker and Cotman, 2021). Emerging evidence suggested that accumulated oxidative stress may be one of the key mechanisms causing cognitive dysfunction and neurodegenerative diseases (Birla et al., 2020). Our previous studies showed that LZJSF exhibited antioxidant activity *in vitro* through decreasing 1,1-Diphenyl-2-picrylhydrazyl free radical ($DPPH^{\cdot}$) free radical, superoxide anion (O_2^{-}) radical scavenging, as well as ferric reducing antioxidant power (FRAP) at chemical levels and reducing MDA and reactive oxygen species (ROS) at PC12 cell level (Yan et al., 2020). Consistent with our previous results, we also found that HLZJSF effectively reduced the high levels of oxidative stress in D-gal-induced aging rats by increasing the activity of antioxidant enzymes SOD, CAT, T-AOC and GSH-Px in the brain and decreasing the accumulation of toxic oxidation products MDA, which was helpful for delaying the progress of cognitive ability and preventing neurodegenerative diseases. In addition, the effects of HLZJSF on improving learning-memory and regulating oxidative stress indexes were superior to those of LLZJSF. Thus, the mechanism study of HLZJSF on delaying the progress of cognitive ability was further analyzed.

4.2. HLZJSF regulated the metabolic abnormalities of serum and urine in D-gal-induced aging rats

Cognitive dysfunction caused by aging was closely related to the body's metabolism (Kondoh et al, 2020). In the present study, D-Glutamine and D-glutamate, alanine, aspartate and glutamate, arginine and proline metabolism, and arginine biosynthesis were considered as the significant pathways associated with the regulatory effects of HLZJSF based on the results of the serum and urine metabolomics.

D-Glutamine and D-glutamate metabolism made an important impact on the process of aging (Zou et al., 2010). Glutamate, an important excitatory neurotransmitter, was involved in a variety of age-related neurodegenerative diseases (Cox et al., 2022). In addition, the dysregulation of glutamate signaling could lead to cognitive ability (Chang et al., 2020). An increasing body of research indicated the significant involvement of arginine and proline metabolism in the aging process (Phang, 2019, Zhao, et al., 2020). In the present study, three important metabolites, including arginine, glutamate and creatinine, were involved in the disturbances of those pathways induced by D-gal. Arginine served as the central substrate in the pathway and acted as the exclusive precursor of nitric oxide (NO). NO led to the generation of reactive oxygen species and was closely associated with arginine content during the natural aging process (Shannon et al., 2022). In our study, arginine and glutamate levels were elevated in the serum of D-gal-induced aging rats compared to the Control group. Meanwhile, treatment with HLZJSF significantly reduced serum arginine and glutamate levels.

In addition, isoleucine, leucine and valine were branched-chain

amino acids that played a key physiological role in metabolism and aging (Le Couteur et al., 2020). (Trautman et al., 2022) had reported that reducing branched-chain amino acids could delay aging and prevent aging-related diseases. Our study showed that a significant increase in serum isoleucine, leucine, and valine in rats induced by D-gal, aligning with the finding of a previous report (Juricic et al., 2020). HLZJSF treatment returned the levels of branched-chain amino acids. In conclusion, HLZJSF might ameliorate the imbalanced metabolic disorders of amino acids and oxidative stress, which contributed to improve and alleviate memory and cognitive abilities of D-gal-induced aging rats.

4.3. HLZJSF regulated gut microbiota dysbiosis in D-gal-induced aging rats

The gut microbiota had been referred to as the "forgotten organ" due to its crucial role in maintaining bodily homeostasis and contributing to improve cognitive ability (Liu et al., 2022a). In 2018, Lu and his colleagues (Lu et al., 2018) showed significant deficits of memory in germ-free mice, which supported the important role of the microbiota in memory development. An increasing body of research indicated that the age-related changes in the gut microbiota composition include a decline in microbiota diversity, a decrease in the abundance of glycolytic bacteria and an increase in proteolytic bacteria (Vaiserman et al., 2017). In the present study, HLZJSF significantly increased the α-diversity and β-diversity, indicating that HLZJSF could alleviate the disorders of gut microbiota induced by D-gal. Therefore, we also explored the effect of HLZJSF on the gut microbiota to reveal the molecular mechanisms by which HLZJSF mitigated cognitive ability. *Firmicutes* and *Bacteroidetes* were enriched in elderly people gut microbiota, and smaller proportions of *Proteobacteria, Actinobacteria* and *Verrucomicrobia* were observed (Białecka-Dębek et al., 2021). *Bacteroidetes* were one of the most abundant in gut bacteria and were closely related to aging (Luo et al., 2020). In this study, HLJZSF could largely restored the gut microbiota structures, decreased the relative abundance of *Bacteroidetes* and increased the relative abundance of *Firmicutes* and the ratio of F/B. Notably, we also observed a significantly reduction in the abundance of *Proteobacteria* in D-gal-induced aging rats, which was consistent with the research report (Shin et al., 2015). Conversely, HLZJSF treatment recovered the abundance of Proteobacteria. Importantly, the six of 12 differential taxa on the family level and five of 12 on the genus level associated with HLZJSF belonged to phylum Firmicutes and Actinobacteria. These results suggested that HLZJSF may play a beneficial role in aging prevention by regulating gut microbiota dysregulation.

Correlation analysis further verified that the changed abundance of gut microbiota was connected with cognitive ability. Previous studies suggested that gut microbiota dysbiosis was associated with cognitive ability during aging (Atienza et al., 2018, Yang et al., 2019). Hoffman et al. found that decreased *Bacteroidetes* were associated with impaired cognitive ability in aging mice (Hoffman et al., 2017). Consistently, we found that *Bacteroidetes* showed significant positive associations with swimming speed, suggesting HLZJSF improved cognitive ability by regulating *Bacteroidetes*. Previous research showed that *Clostridium* was a harmful bacterium to health (Amrane et al. 2018). In the present study, *Clostridium* was negatively correlated with swimming speed, which was consistent with previous studies (Xie et al., 2020). These results suggested that HLZJSF improved cognitive ability by regulating gut microbiota.

Experimental evidence suggested that a complex association between commensal gut microbiota and oxidative indexes (Sun et al., 2022). Especially, the main altered microbiota taxa belonging to the phylum level including *Firmicutes*, *Bacteroidetes*, *Actinobacteria* and *Proteobacteria*, which were highly correlated with the oxidative indexes. Previous studies had reported that the higher abundance of *Bacteroidetes* could increase intestinal wall thickness to reduce oxidative stress (Xie et al., 2020). In the present study, we found *Bacteroidetes* exhibited significant positive correlations with brain SOD, GSH-Px and T-AOC, while exhibiting negative correlations with brain MDA. Importantly, the serum SOD, CAT and T-AOC levels were enhanced after administration of HLZJSF. *Unclassified_Lachnospiraceae* (members of *Firmicutes*) was one of the important microbiotas at the genus level and was closely related to aging (Sheng et al., 2022). Previous studies had reported that supplementation with *unclassified_Lachnospiraceae* could effectively mitigate oxidative stress within the body in aging (Li et al., 2019b), and *unclassified_Lachnospiraceae* was closely related to cognitive impairment (Li et al., 2023b). In consistent, the relative abundance of *unclassified_Lachnospiraceae* was positively correlated with brain SOD and T-AOC. In addition, previous research had showed that *Actinobacteria*, closely related to aging, was one of the major gut microbiotas in D-gal-induced mice (Liu et al., 2023b). Recent studies had reported that *Actinobacteria* were potentially important pathogens in humans and caused oxidative stress to immune function (Barka et al., 2016). Coincidentally, we found that *Actinobacteria* was negatively correlated with brain oxidative indexes (such as GSH-Px, CAT and T-AOC), while an opposite trend with brain MDA was observed in the present study. These results suggested that HLZJSF may play a beneficial role in anti-aging by regulating gut microbiota dysregulation, thereby reduced the high levels of oxidative stress.

In addition, studies had reported that the homeostasis of the gut microflora affected metabolites and led to cognitive ability (Liu et al., 2023b). Recent studies showed that glutamate was a key signaling metabolite which linked gut microbiota to the brain (Zhao et al., 2023). Kadyan et al. found a significant negative correlation between glutamate and *Bacteroides* in an aging mouse model (Kadyan et al., 2023). In line with the previous study, we found that glutamate was significantly associated with *Bacteroides*, *Proteobacteria*, *Firmicutes* and *Actinobacteria*. Previous studies had found that long-term use of probiotics and arginine could treat age-related cognitive ability decline (Joho et al., 2023). In this study, *Bacteroidetes* and *Proteobacteria* showed strong positive associations with serum arginine. These results suggested that HLZJSF treatment ameliorated cognitive ability by improving gut microbiota thereby metabolic disorders in D-gal-induced aging rats. Interestingly, we also found that *Bacteroidetes* and *Unclassified_Lachnospiraceae* showed strong positive associations with branched-chain amino acids (such as leucine, valine, isoleucine), suggesting HLZJSF could improve cognitive ability in D-gal-induced aging rats by effectively regulating gut microbiota and branched-chain amino acid metabolism. However, the mechanism needed to be studied in the further research.

Moreover, LZJSF extracts were rich in quercetin- and kaempferol-type flavonoids. According to *in vitro* fecal incubations study, LZJSF were easily metabolized to their aglycones (quercetin and kaempferol) via deglycosylation and dehydroxylation reactions (Yan et al., 2020), which might support the finding here that LZJSF mitigated aging-associated cognitive ability via the microbiota-gut-brain axis. Moreover, a number of metabolites originating from LZJSF have been reported to be have a higher antioxidant activity and better absorption than flavonoid glucosides, suggesting that the LZJSF metabolites may also participate in the anti-aging effect of LZJSF.

Hence, we have preliminarily proven that HLZJSF might improve cognitive impairment and delay brain aging by regulating the disturbance of gut microbiota through the "microbiota-gut-brain" axis to affect amino acid and regulate oxidative stress (Fig. 7). In addition, the current study had some limitations. In gut microbiota study, the group size of rat was small, therefore, the validations at the genes and protein levels were required for a further study. More work (the functions of affected genes) needed to be done to completely clarify the mechanism underlying the antiaging effect of LZJSF.

5. Conclusion

In summary, in the study, we demonstrated that LZJSF alleviated the cognitive ability by the Morris water maze test and the oxidative stress by upregulating the contents of SOD, GSH-Px, CAT and T-AOC in the

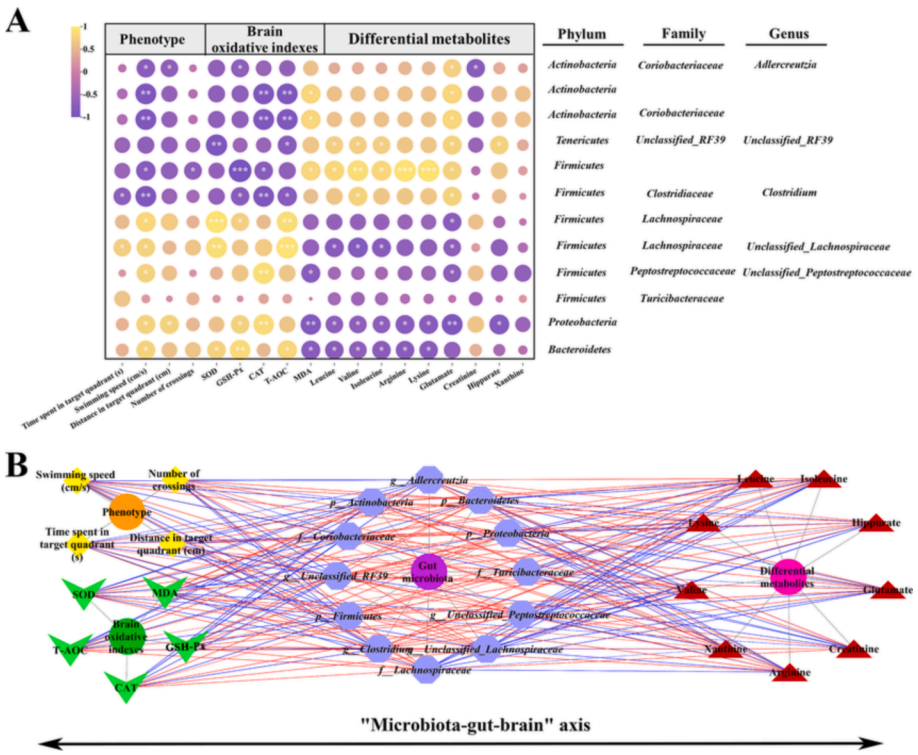

Fig. 6. (A) Spearman correlation analysis of gut microbiota with aging–related features. Purple and yellow colors represent negative and positive correlations, respectively; *P* value, the depth of color and the size of the circle indicate the degree of correlation; (B) The correlation network of differential gut bacteria and phenotype, brain oxidative indexes, and differential metabolites. Yellow: phenotype; Green: brain oxidative indexes; Purple: differential gut bacteria; Red: differential metabolites; The blue line: negative correlation; The red line: positive correlation. The strength of correlation increases proportionally with the thickness of the line. Significant correlations were marked by $*P < 0.05$, $**P < 0.01$ and $***P < 0.001$.

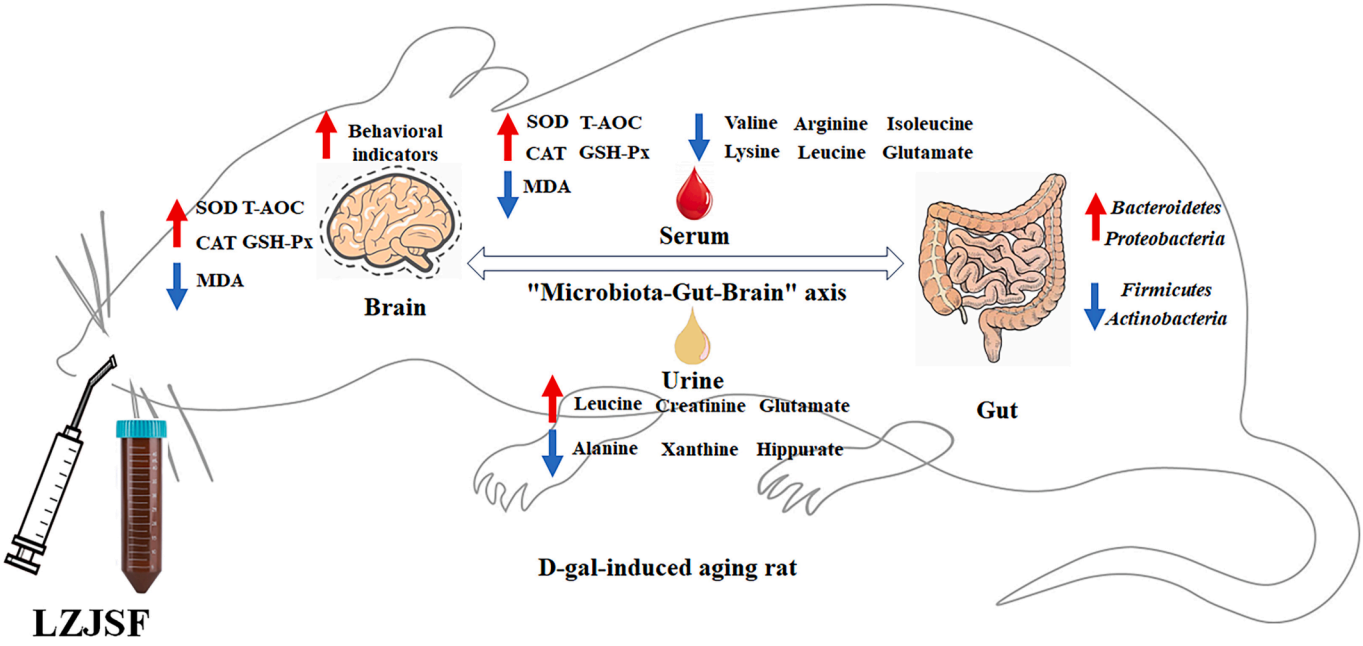

Fig. 7. The scheme of the anti-aging effects of LZJSF from the perspective of the "microbiota-gut-brain" axis.

serum and brain, and downregulating the content of MDA in the brain. D-Glutamine and D-glutamate metabolism, alanine, aspartate and glutamate metabolism, arginine biosynthesis and arginine and proline metabolism, were considered as the significant pathway associated with the regulatory effects of HLZJSF through integrated serum and urine metabolomics. In addition, 16S rRNA sequencing technology showed that HLZJS could modulate the composition and structure of gut microbiota in altered by D-gal through descend the ratio of *Firmicutes/Bacteroidetes*, *Firmicutes*, *Actinobacteria* and increase the relative abundance of *Bacteroidetes* and *Proteobacteria*. The beneficial effects resulted from the regulation of the disturbance of gut microbiota through the "microbiota-gut-brain" axis to affect amino acid metabolism and

regulate oxidative stress.

CRediT authorship contribution statement

Yu Tao: Data curation, Conceptualization, Formal analysis, Writing – original draft. **Cai Fu:** Writing – original draft, Data curation, Conceptualization. **Huizhi Du:** Supervision. **Chenhui Du:** Funding acquisition, Methodology. **Yan Yan:** Project administration, Writing – review & editing.

Declaration of Competing Interest

The authors declare that they have no known competing financial interests or personal relationships that could have appeared to influence the work reported in this paper.

Acknowledgements

This work was supported by Key laboratory of Effective Substances Research and Utilization in TCM of Shanxi province (No. 201605D111004), the Innovation Project for Graduate Students in Shanxi Province (2023KY144), Key Laboratory of Chemical Biology and Molecular Engineering of Ministry of Education of Shanxi University (202105D121009), the Central Guide Local Science and Technology Development Fund Project of Shanxi Provincial Science and Technology Department (YDZJSX2021C025), and the Scientific and Technology Innovation Capability Cultivation Program by Shanxi University of Chinese Medicine (2021PN-QN-07).

Appendix A. Supplementary data

Supplementary data to this article can be found online at https://doi.org/10.1016/j.arabjc.2023.105591.

References

Ahmed, N., Biagi, E., Nylund, L., et al., 2010. Through ageing, and beyond: gut microbiota and inflammatory status in seniors and centenarians. PLoS One 5, e10667.

Amrane, S., Bachar, D., Lagier, J.C., et al., 2018. Clostridium scindens Is Present in the Gut Microbiota during Clostridium difficile Infection: a Metagenomic and Culturomic Analysis. J. Clin. Microbiol. 56, e01663–e10717. https://doi.org/10.1128/JCM.01663-17.

Atienza, M., Ziontz, J., Cantero, J.L., 2018. Low-grade inflammation in the relationship between sleep disruption, dysfunctional adiposity, and cognitive decline in aging. Sleep Med. Rev. 42, 171–183. https://doi.org/10.1016/j.smrv.2018.08.002.

Bai, L., Cui, X., Cheng, N., et al., 2017. Hepatoprotective standardized EtOH-water extract of the leaves of Ziziphus jujuba. Food Funct. 8, 816–822. https://doi.org/10.1039/c6fo01690a.

Barka, E.A., Vatsa, P., Sanchez, L., et al., 2016. Taxonomy, physiology, and natural products of *Actinobacteria*. Microbiol. Mol. Biol. Rev. 80, 1–43. https://doi.org/10.1128/MMBR.00019-15.

Białecka-Dębek, A., Granda, D., Szmidt, M.K., et al., 2021. Gut microbiota, probiotic interventions, and cognitive function in the elderly: A Review of Current Knowledge. Nutrients. 13, 2514. https://doi.org/10.3390/nu13082514.

Birla, H., Minocha, T., Kumar, G., et al., 2020. Role of Oxidative Stress and Metal Toxicity in the Progression of Alzheimer's Disease. Curr. Neuropharmacol. 18, 552–562. https://doi.org/10.2174/1570159X18666200122122512.

Chang, C.H., Lin, C.H., Lane, H.Y., 2020. d-glutamate and Gut Microbiota in Alzheimer's Disease. Int. J. Mol. Sci. 21, 2676. https://doi.org/10.3390/ijms21082676.

Chen, L., Garmaeva, S., Zhernakova, A., et al., 2018. A system biology perspective on environment-host-microbe interactions. Hum. Mol. Genet. 27, R187–R194. https://doi.org/10.1093/hmg/ddy137.

Cox, M.F., Hascup, E.R., Bartke, A., et al., 2022. Friend or Foe? Defining the Role of Glutamate in Aging and Alzheimer's Disease. Front. Aging. 3, 929474 https://doi.org/10.3389/fragi.2022.929474.

Du, C., Yan, Y., Shen, C., et al., 2020. Comparative pharmacokinetics of six major compounds in normal and insomnia rats after oral administration of Ziziphi Spinosae Semen aqueous extract. J. Pharm. Anal. 10, 385–395. https://doi.org/10.1016/j.jpha.2020.03.003.

Guo, S., Duan, J.A., Tang, Y., et al., 2011. Simultaneous qualitative and quantitative analysis of triterpenic acids, saponins and flavonoids in the leaves of two Ziziphus species by HPLC-PDA-MS/ELSD. J. Pharm. Biomed. Anal. 56, 264–270. https://doi.org/10.1016/j.jpba.2011.05.025.

Guo, S., Duan, J.A., Qian, D., et al., 2013. Hydrophilic interaction ultra-high performance liquid chromatography coupled with triple quadrupole mass spectrometry for determination of nucleotides, nucleosides and nucleobases in Ziziphus plants. J. Chromatogr. A. 1301, 147–155. https://doi.org/10.1016/j.chroma.2013.05.074.

Hoffman, J.D., Parikh, I., Green, S.J., et al., 2017. Age Drives Distortion of Brain Metabolic, Vascular and Cognitive Functions, and the Gut Microbiome. Front Aging Neurosci. 9, 298. https://doi.org/10.3389/fnagi.2017.00298.

Ionescu-Tucker, A., Cotman, C.W., 2021. Emerging roles of oxidative stress in brain aging and Alzheimer's disease. Neurobiol. Aging. 107, 86–95. https://doi.org/10.1016/j.neurobiolaging.2021.07.014.

Joho, D., Takahashi, M., Suzuki, T., et al., 2023. Probiotic treatment with Bifidobacterium animalis subsp. lactis LKM512 + arginine improves cognitive flexibility in middle-aged mice. Brain Commun. 5, fcad311. https://doi.org/10.1093/braincomms/fcad311.

Juricic, P., Grönke, S., Partridge, L., 2020. Branched-chain amino acids have equivalent effects to other essential amino acids on lifespan and aging-related traits in drosophila. J. Gerontol. A Biol. Sci. Med. Sci. 75, 24–31. https://doi.org/10.1093/gerona/glz080.

Kadyan, S., Park, G., Wang, B., et al., 2023. Dietary fiber modulates gut microbiome and metabolome in a host sex-specific manner in a murine model of aging. Front. Mol. Biosci. 10, 1182643. https://doi.org/10.3389/fmolb.2023.1182643.

Kondoh, H., Kameda, M., Yanagida, M., 2020. Whole Blood Metabolomics in Aging Research. Int. J. Mol. Sci. 22, 175. https://doi.org/10.3390/ijms22010175.

Le Couteur, D.G., Solon-Biet, S.M., Cogger, V.C., et al., 2020. Branched chain amino acids, aging and age-related health. Ageing Res. Rev. 64, 101198 https://doi.org/10.1016/j.arr.2020.101198.

Li, T., Chen, S., Feng, T., et al., 2016. Rutin protects against aging-related metabolic dysfunction. Food Funct. 7, 1147–1154. https://doi.org/10.1039/c5fo01036e.

Li, Y., Chen, Y., Fan, Y., et al., 2023b. Dynamic network modeling of gut microbiota during Alzheimer's disease progression in mice. Gut Microbes. 15, 2172672. https://doi.org/10.1080/19490976.2023.2172672.

Li, J., Wu, T., Li, N., et al., 2019b. Bilberry anthocyanin extract promotes intestinal barrier function and inhibits digestive enzyme activity by regulating the gut microbiota in aging rats. Food Funct. 10, 333–343. https://doi.org/10.1039/c8fo01962b.

Li, C., Zhang, J., Wu, R., et al., 2019a. A novel strategy for rapidly and accurately screening biomarkers based on ultraperformance liquid chromatography-mass spectrometry metabolomics data. Anal. Chim. Acta. 1063, 47–56. https://doi.org/10.1016/j.aca.2019.03.012.

Li, M., Zhang, C., Xiao, X., et al., 2023a. Theaflavins in black tea mitigate aging-associated cognitive dysfunction via the microbiota–gut–brain axis. J. Agric. Food Chem. 71, 2356–2369. https://doi.org/10.1021/acs.jafc.2c06679.

Liu, B., Chen, B., Yi, J., et al., 2022a. Liuwei dihuang decoction alleviates cognitive dysfunction in mice with D-galactose-induced aging by regulating lipid metabolism and oxidative stress via the microbiota-gut-brain axis. Front. Neurosci. 16, 949298 https://doi.org/10.3389/fnins.2022.949298.

Liu, Z., Fayyaz, S., Zhao, D., et al., 2023b. Polygonatum sibiricum polysaccharides improve cognitive function in D-galactose-induced aging mice by regulating the microbiota-gut-brain axis. J. Funct. Foods. 103, 105476 https://doi.org/10.1016/j.jff.2023.105476.

Liu, W., He, K., Wu, D., et al., 2022b. Natural dietary compound xanthohumol regulates the gut microbiota and its metabolic profile in a mouse model of Alzheimer's disease. Molecules. 27, 1281. https://doi.org/10.3390/molecules27041281.

Liu, Y., Lian, X., Qin, X., 2023a. Bile acid metabolism involved into the therapeutic action of Xiaojianzhong Tang via gut microbiota to treat chronic atrophic gastritis in rats. Phytomedicine. 109, 154557 https://doi.org/10.1016/j.phymed.2022.154557.

Lu, J., Synowiec, S., Lu, L., et al., 2018. Microbiota influence the development of the brain and behaviors in C57BL/6J mice. PLoS One. 13, e0201829.

Luo, D., Chen, K., Li, J., et al., 2020. Gut microbiota combined with metabolomics reveals the metabolic profile of the normal aging process and the anti-aging effect of FuFang Zhenshu TiaoZhi (FTZ) in mice. Biomed. Pharmacother. 121, 109550. https://doi.org/10.1016/j.biopha.2019.109550.

Mifflin, M.A., Winslow, W., Surendra, L., et al., 2021. Sex differences in the IntelliCage and the Morris water maze in the APP/PS1 mouse model of amyloidosis. Neurobiol. Aging. 101, 130–140. https://doi.org/10.1016/j.neurobiolaging.2021.01.018.

Mou, Y., Du, Y., Zhou, L., et al., 2022. Gut microbiota interact with the brain through systemic chronic inflammation: implications on neuroinflammation, neurodegeneration, and aging. Front. Immunol. 13, 796288 https://doi.org/10.3389/fimmu.2022.796288.

Phang, J.M., 2019. Proline Metabolism in cell regulation and cancer biology: recent advances and hypotheses. Antioxid. Redox. Signal. 30, 635–649. https://doi.org/10.1089/ars.2017.7350.

Ruan, Q., Liu, F., Gao, Z., et al., 2013. The anti-inflamm-aging and hepatoprotective effects of huperzine A in D-galactose-treated rats. Mech. Ageing Dev. 134, 89–97. https://doi.org/10.1016/j.mad.2012.12.005.

Shannon, O.M., Clifford, T., Seals, D.R., et al., 2022. Nitric oxide, aging and aerobic exercise: Sedentary individuals to Master's athletes. Nitric Oxide. 125–126, 31–39. https://doi.org/10.1016/j.niox.2022.06.002.

Sheng, K., Yang, J., Xu, Y., et al., 2022. Alleviation effects of grape seed proanthocyanidin extract on inflammation and oxidative stress in a D-galactose-induced aging mouse model by modulating the gut microbiota. Food Funct. 13, 1348–1359. https://doi.org/10.1039/d1fo03396d.

Shin, N.R., Whon, T.W., Bae, J.W., 2015. Proteobacteria: microbial signature of dysbiosis in gut microbiota. Trends Biotechnol. 33, 496–503. https://doi.org/10.1016/j.tibtech.2015.06.011.

Sun, X., Yu, J., Wang, Y., et al., 2022. Flaxseed oil ameliorates aging in d-galactose induced rats via altering gut microbiota and mitigating oxidative damage. J. Sci. Food. Agric. 102, 6432–6442. https://doi.org/10.1002/jsfa.12010.

Sun, W., Zhu, J., Qin, G., et al., 2023. Lonicera japonica polysaccharides alleviate D-galactose-induced oxidative stress and restore gut microbiota in ICR mice. Int. J. Biol. Macromol. 245, 125517 https://doi.org/10.1016/j.ijbiomac.2023.125517.

Trautman, M.E., Richardson, N.E., Lamming, D.W., 2022. Protein restriction and branched-chain amino acid restriction promote geroprotective shifts in metabolism. Aging Cell. 21, e13626.

Vaiserman, A.M., Koliada, A.K., Marotta, F., 2017. Gut microbiota: A player in aging and a target for anti-aging intervention. Ageing Res. Rev. 35, 36–45. https://doi.org/10.1016/j.arr.2017.01.001.

Xie, D., Jiang, L., Lin, Y., et al., 2020. Antioxidant activity of selenium-enriched Chrysomyia megacephala (Fabricius) larvae powder and its impact on intestinal microflora in D-galactose induced aging mice. BMC Complement. Med. Ther. 20, 264. https://doi.org/10.1186/s12906-020-03058-4.

Yan, Y., Fu, C., Cui, X., et al., 2020. Metabolic profile and underlying antioxidant improvement of Ziziphi Spinosae Folium by human intestinal bacteria. Food Chem. 320, 126651 https://doi.org/10.1016/j.foodchem.2020.126651.

Yang, Y.C., Lin, H.Y., Su, K.Y., et al., 2012. Rutin, a flavonoid that is a main component of saussurea involucrata, attenuates the senescence effect in D-galactose aging mouse model. Evid. Based Complement. Alternat. Med. 2012, 980276 https://doi.org/10.1155/2012/980276.

Yang, X., Yu, D., Xue, L., et al., 2019. Probiotics modulate the microbiota-gut-brain axis and improve memory deficits in aged SAMP8 mice. Acta Pharm. Sin. B. 10, 475–487. https://doi.org/10.1016/j.apsb.2019.07.001.

Zhang, R., Chen, J., Shi, Q., et al., 2014. Phytochemical analysis of Chinese commercial Ziziphus jujube leaf tea using high performance liquid chromatography–electrospray ionization-time of flight mass spectrometry. Food Res. Int. 56, 47–54. https://doi.org/10.1016/j.foodres.2013.12.019.

Zhao, Q., Chen, J., Wu, M., et al., 2023. Microbiota from healthy mice alleviates cognitive decline via reshaping the gut-brain metabolic axis in diabetic mice. Chem. Biol. Interact. 382, 110638 https://doi.org/10.1016/j.cbi.2023.110638.

Zhao, S.J., Liu, X.J., Tian, J.S., et al., 2020. Effects of guilingji on aging rats and its underlying mechanisms. Rejuvenation Res. 23, 138–149. https://doi.org/10.1089/rej.2018.2118.

Zou, J., Wang, Y.X., Dou, F.F., et al., 2010. Glutamine synthetase down-regulation reduces astrocyte protection against glutamate excitotoxicity to neurons. Neurochem. Int. 56, 577–584. https://doi.org/10.1016/j.neuint.2009.12.021.